Acta Crystallographica Section D
Biological Crystallography
ISSN 0907-4449

Structural analysis of malaria-parasite lysyl-tRNA synthetase provides a platform for drug development

Sameena Khan,[a] Ankur Garg,[a] Noelia Camacho,[b] Jason Van Rooyen,[d] Anil Kumar Pole,[a] Hassan Belrhali,[d] Lluis Ribas de Pouplana,[b,c] Vinay Sharma[e] and Amit Sharma[a]*

[a]Structural and Computational Biology Group, International Centre for Genetic Engineering and Biotechnology (ICGEB), Aruna Asaf Ali Road, New Delhi 110 067, India, [b]Institute for Research in Biomedicine (IRB Barcelona), c/Baldiri Reixac 10, Barcelona, 08028, Catalonia, Spain, [c]Catalan Institution for Research and Advanced Studies (ICREA), Pg. Lluís Companys 23, Barcelona, 08010, Catalonia, Spain, [d]European Molecular Biology Laboratory (EMBL), 6 Rue Jules Horowitz, BP 181, F-38042 Grenoble, France, and [e]Department of Bioscience and Biotechnology, Banasthali Vidyapith University, Banasthali, Rajasthan 304 022, India

Correspondence e-mail: amit.icgeb@gmail.com

Received 13 October 2012
Accepted 18 January 2013

PDB Reference: *Pf* LysRS, 4h02

Aminoacyl-tRNA synthetases are essential enzymes that transmit information from the genetic code to proteins in cells and are targets for antipathogen drug development. Elucidation of the crystal structure of cytoplasmic lysyl-tRNA synthetase from the malaria parasite *Plasmodium falciparum* (*Pf*LysRS) has allowed direct comparison with human LysRS. The authors' data suggest that *Pf*LysRS is dimeric in solution, whereas the human counterpart can also adopt tetrameric forms. It is shown for the first time that *Pf*LysRS is capable of synthesizing the signalling molecule Ap4a (diadenosine tetraphosphate) using ATP as a substrate. The *Pf*LysRS crystal structure is in the apo form, such that binding to ATP will require rotameric changes in four conserved residues. Differences in the active-site regions of parasite and human LysRSs suggest the possibility of exploiting *Pf*LysRS for selective inhibition. These investigations on *Pf*LysRS further validate malarial LysRSs as attractive antimalarial targets and provide new structural space for the development of inhibitors that target pathogen LysRSs selectively.

1. Introduction

Malaria remains a major challenge to public health despite global efforts to fight it (World Health Organization, 2011). *Plasmodium falciparum*, the parasite responsible for most morbidity and mortality from malaria, has developed resistance to many drugs in clinical use (World Health Organization, 2011). Therefore, detailed structure–function studies of crucial malaria-parasite proteins are critical in furthering the identification of new drug targets. The protein-translation machinery of the malaria parasite is a vital engine which is increasingly being considered as a good target for the development of antimalarials (Bhatt *et al.*, 2009, 2011; Istvan *et al.*, 2011; Jackson *et al.*, 2011; Hoepfner *et al.*, 2012). Aminoacyl-tRNA synthetases (aaRSs) attach specific amino acids to cognate tRNA molecules and are pivotal in determining how genetic code is interpreted (Ibba & Söll, 2000; O'Donoghue & Luthey-Schulten, 2003). Sequence similarity and structural studies have revealed that it is possible to divide aaRSs into two classes, where each class shares sequence motifs and a similar topology in the catalytic domain (Ibba & Söll, 2000; O'Donoghue & Luthey-Schulten, 2003). Class I enzymes contain two conserved sequences, HIGH and KMSKS, shown to be involved in ATP binding (Ibba & Söll, 2000; O'Donoghue & Luthey-Schulten, 2003). In contrast, class II enzymes are characterized by three conserved sequence motifs (1, 2 and

3) which are involved in dimerization and amino-acid activation (Ibba & Söll, 2000; O'Donoghue & Luthey-Schulten, 2003). In eukaryotes and most prokaryotes, lysyl-tRNA synthetases (LysRSs) belong to the class II family of aaRSs, but in some archaea and bacteria lysyl-tRNA charging activity is associated with a protein containing the conserved motifs characteristic of class I enzymes (Ibba *et al.*, 1997, 1999; Ibba & Söll, 2000; O'Donoghue & Luthey-Schulten, 2003). LysRS is the only example of an aaRS activity catalyzed by both classes of aaRS enzymes (Ibba *et al.*, 1997, 1999). Although the global and local architectures of LysRS I and LysRS II are fundamentally different, it seems that the two LysRSs approach the tRNA acceptor helix from opposite sides; in a sense, their strategies to recognize $tRNA^{Lys}$ as well as L-lysine have similarities (Terada *et al.*, 2002). This strongly suggests functional convergence of the two unrelated LysRS I and LysRS II enzymes. Human LysRS has other physiological roles in addition to aminoacylation (Park *et al.*, 2005). For example, full-length human LysRS functions as a cytokine that binds to macrophages and peripheral blood mononuclear cells to activate their migration and TNF-α production (Park *et al.*, 2005). In addition to its immunological properties, human LysRS and others are able to synthesize diadenosine polyphosphate (Ap4a; Lee *et al.*, 1983; Varshavsky, 1983; Yannay-Cohen *et al.*, 2009).

Crystal structure analysis of human LysRS indicated the possibility of tetrameric LysRS in solution (Guo *et al.*, 2008). Later, it was speculated that the tetramer interface of LysRS (α4) is exploited by the p38 dimer (β2) to produce an $\alpha2\beta2$ subcomplex in the MSC (multisynthetase complex), which suggested that LysRS might be bound to MSC in an $\alpha2\beta2$ form (Fang *et al.*, 2011). However, the oligomeric states in crystal structures of nonhuman LysRSs suggest dimeric forms. The critical distinction between dimeric and tetrameric forms of LysRSs is therefore of considerable importance as it has implications for enzyme mechanism. Finally, a recent study discovered that the fungal secondary metabolite cladosporin is a potent inhibitor of both the blood and liver stages of malaria *via* its action on *Pf*LysRS (Hoepfner *et al.*, 2012). Here, we present the 2.9 Å resolution crystal structure of *Pf*LysRS in an apo (unliganded) form. We show that *Pf*LysRS has the canonical catalytic and anticodon-binding domain and that this protein exists as a dimer (only) in solution. We show that *Pf*LysRS resides in the parasite cytoplasm both in *P. falciparum* cultures and in *ex vivo P. yoelii* parasites. The localization of *Pf*LysRS in the parasite cytoplasm strongly suggests that this protein contributes to the cytoplasmic protein-translation process and not to the translation of proteins in the parasite apicoplast. This is also the first study that provides evidence of diadenosine tetraphosphate (Ap4a) production by the malarial enzyme *Pf*LysRS, an observation with potential implications for malarial pathogenesis. Our in-depth structural analysis of *Pf*LysRS suggests key differences in the side-chain conformations within the ATP-binding pockets of the human, bacterial and *Pf*LysRS structures. Our detailed comparisons of LysRS structures in apo and ligand-bound forms from multiple organisms provide mechanistic details of ATP docking in the *Pf*LysRS active site. Our work therefore provides valuable information for structure-based drug development against this family of enzymes.

2. Materials and methods

2.1. Molecular cloning, expression and purification

Protein sequences were accessed from the PlasmoDB *Plasmodium* Genomics Resource (http://www.PlasmoDB.com; Bhal *et al.*, 2003). The *Pf*LysRS gene contains a sequence of unknown function at its N-terminus from residues 1 to 76; this region is specific to *Pf*LysRS and shows no sequence similarity to known domains. A gene construct of *Pf*LysRS (*PF*13_0262) without the N-terminal sequence and encompassing residue 77 to the end was designed for optimal expression in *Escherichia coli*. The construct was subcloned in pETM-41 (MBP with His tag) with *Nco*I and *Kpn*I restriction sites. Protein expression was induced by adding 0.5 m*M* isopropyl β-D-1-thiogalactopyranoside (IPTG) to cells grown at 310 K for 4 h; the cells were then grown for 20 h post-induction at 291 K. The cells were harvested by centrifugation at 5000*g* for 15 min. The bacterial pellet was suspended in a buffer consisting of 50 m*M* Tris–HCl pH 8.0, 200 m*M* NaCl, 10 m*M* β-mercaptoethanol (βMe), 15%(*v*/*v*) glycerol, 0.1 mg ml^{-1} lysozyme and EDTA-free protease-cocktail inhibitor (Roche). The cells were lysed by sonication and cleared by centrifugation at 20 000*g* for 45 min. The cleared *Pf*LysRS supernatant was applied onto amylose beads (GE Healthcare). The MBP-*Pf*LysRS fusion protein was eluted with 10 m*M* maltose and dialyzed in 50 m*M* Tris–HCl pH 8.0, 200 m*M* NaCl, 10 m*M* βMe, 1 m*M* DTT, 0.5 m*M* EDTA. The tag was removed by incubation with TEV protease at 293 K for 24 h. Cleaved *Pf*LysRS protein was concentrated using a 10 kDa cutoff Centricon centrifugal device (Millipore) and was purified by gel-filtration chromatography on an S200 analytical gel-filtration column (GE Biosciences). Pure fractions were checked by SDS–PAGE and those containing only *Pf*LysRS were pooled and buffer-exchanged in 50 m*M* Tris–HCl pH 8.0, 200 m*M* NaCl, 10 m*M* βMe for crystallization of apo and derivative forms. Before crystallization, 10 m*M* ATP and 2 m*M* L-lysine were added. The protein was concentrated to 13.5 mg ml^{-1} and stored at 193 K.

2.2. Production of polyclonal antibodies and expression analysis

Polyclonal antibodies were raised in rabbits against highly purified recombinant *Pf*LysRS protein. For Western blot analysis, parasites in asynchronous *P. falciparum* cultures were released from infected RBCs (red blood cells) by 0.05%(*w*/*v*) saponin lysis and pellets were washed in phosphate-buffered saline (PBS). The composition of 1× PBS was 8 g NaCl, 0.2 g KCl, 1.44 g Na_2HPO_4, 0.24 g KH_2PO_4 pH 7.4. Parasites were lysed by three rounds of freeze–thawing in RIPA buffer [50 m*M* Tris–HCl, 150 m*M* NaCl, 1 m*M* EDTA, 1%(*v*/*v*) NP40 (nonyl phenoxypolyethoxylethanol), 0.1%(*w*/*v*) SDS, 1%(*w*/*v*) sodium deoxycholate pH 7.4] containing protease-inhibitor

cocktail. Lysates were centrifuged and supernatants were separated on SDS–PAGE. Proteins were transferred to nitrocellulose membrane and blots were probed using specific primary antibodies and secondary alkaline phosphatase-conjugated antibodies (1:1500 dilutions). Bands were visualized using an ECL detection kit and parasite-expressed *Pf*LysRS was probed using antibodies generated against recombinant *Pf*LysRS.

2.3. Immunofluorescence assays using confocal microscopy

An immunofluorescence assay (IFA) was performed as described previously (Tonkin *et al.*, 2004). Cells were washed in PBS and fixed in solution using 4%(*w*/*v*) paraformaldehyde and 0.0075%(*w*/*v*) glutaraldehyde in PBS for 25 min. After a PBS wash, the cells were permeabilized using 0.1%(*v*/*v*) Triton X-100 in PBS for 10 min. After another PBS wash, the cells were treated with 0.1 mg ml^{-1} sodium borohydride in PBS for 10 min. The cells were washed again with PBS, blocked using 3%(*w*/*v*) BSA in PBS for 1 h and incubated overnight with Protein A column-purified rabbit anti-protein IgG antibody (1:250 dilution) at 277 K. The cells were then washed three times with PBS for 10 min each, incubated with Alexa Fluor 488-tagged anti-rabbit secondary antibody for 1 h at room temperature and allowed to settle onto cover slips coated with poly-L-lysine (100 mg ml^{-1}). Finally, the cover slips were washed three times in PBS, mounted in antifade with DAPI reagent (Invitrogen) and sealed. Confocal microscopy was performed on a Nikon Eclipse TE2000U microscope. Pre-immune sera were taken as a negative control.

2.4. Aminoacylation assays

Aminoacylation of tRNA was performed at 310 K in 100 m*M* HEPES pH 7.2, 6 µ*M* lysine, 30 m*M* $MgCl_2$, 30 m*M* KCl, 0.5 m*M* DTT, 5 m*M* ATP, 0.1 mg ml^{-1} BSA, 500 Ci mol^{-1} L-[^{3}H]-lysine and varying concentrations of tRNA transcripts (0.5–20 µ*M*). Reactions were initiated by the addition of pure *Pf*LysRS enzyme and 22 µl samples were spotted onto Whatman 3 mm discs at varying time intervals. Radioactivity was measured by liquid scintillation. *P. falciparum* tRNA^{Lys} obtained by *in vitro* transcription using T7 RNA polymerase (Schulman & Pelka, 1983; Sampson & Uhlenbeck, 1988) was used in aminoacylation assays. Enzyme concentrations were experimentally determined for each tRNA in order to obtain linear velocities (Schulman & Pelka, 1983; Sampson & Uhlenbeck, 1988). *Pf*LysRS enzyme activity was confirmed using pure *Pf*LysRS and *P. falciparum* tRNA^{Lys}. It is evident that the N-terminal extension of 76 residues in *Pf*LysRS is dispensable for aminoacylation activity.

2.5. Size-exclusion chromatography and electron microscopy of *Pf*LysRS

Size-exclusion chromatography was carried out using 100 µl samples (5 mg ml^{-1}) on a Superdex 200 10/300 GL column (GE Healthcare) equilibrated with a solution consisting of 25 m*M* Tris–HCl pH 7.5, 10 m*M* $MgCl_2$, 150 m*M* KCl, 10%(*v*/*v*) glycerol, 1 m*M* DTT. The elution of samples and high-molecular-weight calibration standards (Sigma–Aldrich) at a flow rate of 0.5 ml min^{-1} was monitored at 280 nm using the inline spectrophotometer of an ÄKTA FPLC system (GE Healthcare). Diluted protein solutions (50 µg ml^{-1}) were applied onto copper electron-microscope grids coated with a glow-discharged thin carbon support film (Agar Scientific) before being stained with 2%(*w*/*v*) uranyl acetate solution using the droplet method. Electron micrographs were recorded by a Proscan 2048 × 2048 slow-scan CCD camera at a nominal magnification of 50 000× using a Jeol 1200 EX II microscope operating at 100 kV. Before particle images were selected using *Signature* (Chen & Grigorieff, 2007), micrographs were low-pass filtered (15 Å) and down-sized by a factor of two. Selected images (∼300 particles) were then summed and rotationally averaged before the radial profiles were plotted with *ImageJ* (Abramoff *et al.*, 2004).

2.6. Crystallization, data collection and structure determination

Crystals of *Pf*LysRS were obtained at 293 K by the hanging-drop vapour-diffusion method using 1 µl *Pf*LysRS (13.5 mg ml^{-1}) and 1 µl 0.1 *M* bis-tris pH 6.5, 2%(*v*/*v*) Tascimate pH 6.0, 20%(*w*/*v*) PEG 3350. Plate-shaped single crystals were directly mounted in cooled nitrogen gas at 100 K. X-ray diffraction data were collected using a MAR CCD detector on beamline BM14 of the European Synchrotron Radiation Facility, Grenoble, France. A total of 720 images were collected with 1 min exposure and 0.5° oscillation per frame. The diffraction images were processed and scaled with the *HKL*-2000 program suite (Otwinowski & Minor, 1997). The initial model was built by *AutoBuild* in *PHENIX* (Adams *et al.*, 2010) and was subsequently rebuilt manually using *Coot* (Emsley & Cowtan, 2004). Model refinement was performed using *phenix.refine* in *PHENIX*. All structural superimposition and preparation of figures was carried out using *UCSF Chimera* (Pettersen *et al.*, 2004). For docking, protein structures were prepared using *Prepwizard* from *Prime* v.3.0 (Schrödinger). The structure of cladosporin was drawn using the *Build* module of *LigPrep* (Schrödinger). Superpositioning of *Pf*LysRS on ligand-bound *Hs*LysRS was performed for analysis of adenosine/ATP binding. We also docked cladosporin against *Hs*LysRS to obtain the *Hs*LysRS–cladosporin complex. For docking, a grid was generated at ∼10 Å surrounding the ATP-binding pocket and *Glide*-based (*Glide* v.5.7; Schrödinger) extra-precision docking was performed in flexible mode. The *Glide* scoring function was used to map the contribution of each atom. The radii of gyration of available full-length LysRS structures were calculated using the *MMTSB* toolset. R.m.s.d.s between *Pf*LysRS and all of the available class II LysRS structures in the PDB were calculated using the *DALI* structural alignment software.

2.7. Diadenosine tetraphosphate (Ap4a) formation assay

Ap4a synthesis was monitored at 310 K in 10 µl standard buffer consisting of 20 m*M* phosphate (K_2HPO_4/KH_2PO_4 pH 7.4), 150 m*M* KCl, 5 m*M* $MgCl_2$, 200 m*M* $ZnCl_2$, 1 µl α-[^{32}P]-

ATP (0.5 µCi µl^{-1}), 1 m*M* L-Lys. The reaction was initiated by the addition of a limiting amount of *Pf*LysRS (500 n*M*) and was incubated at 310 K for 3 h. 1 µl of reaction mixture was spotted onto a polyethyleneimine cellulose plate (Merck) and developed based on the size of the nucleobases using 3 *M* ammonium sulfate, 2%(*w*/*v*) EDTA pH 5.5 as described by Bochner & Ames (1982). [^{32}P]-Labelled compounds were visualized using a Typhoon scanner (GE Healthcare).

3. Results and discussion

3.1. *Pf*LysRS expression and localization in the malaria parasite

Specific antibodies were raised against *Pf*LysRS in rabbits and were used to explore the cellular localization of *Pf*LysRS within the malaria parasite. *Pf*LysRS antibodies were also tested against parasite lysates and the quality of the

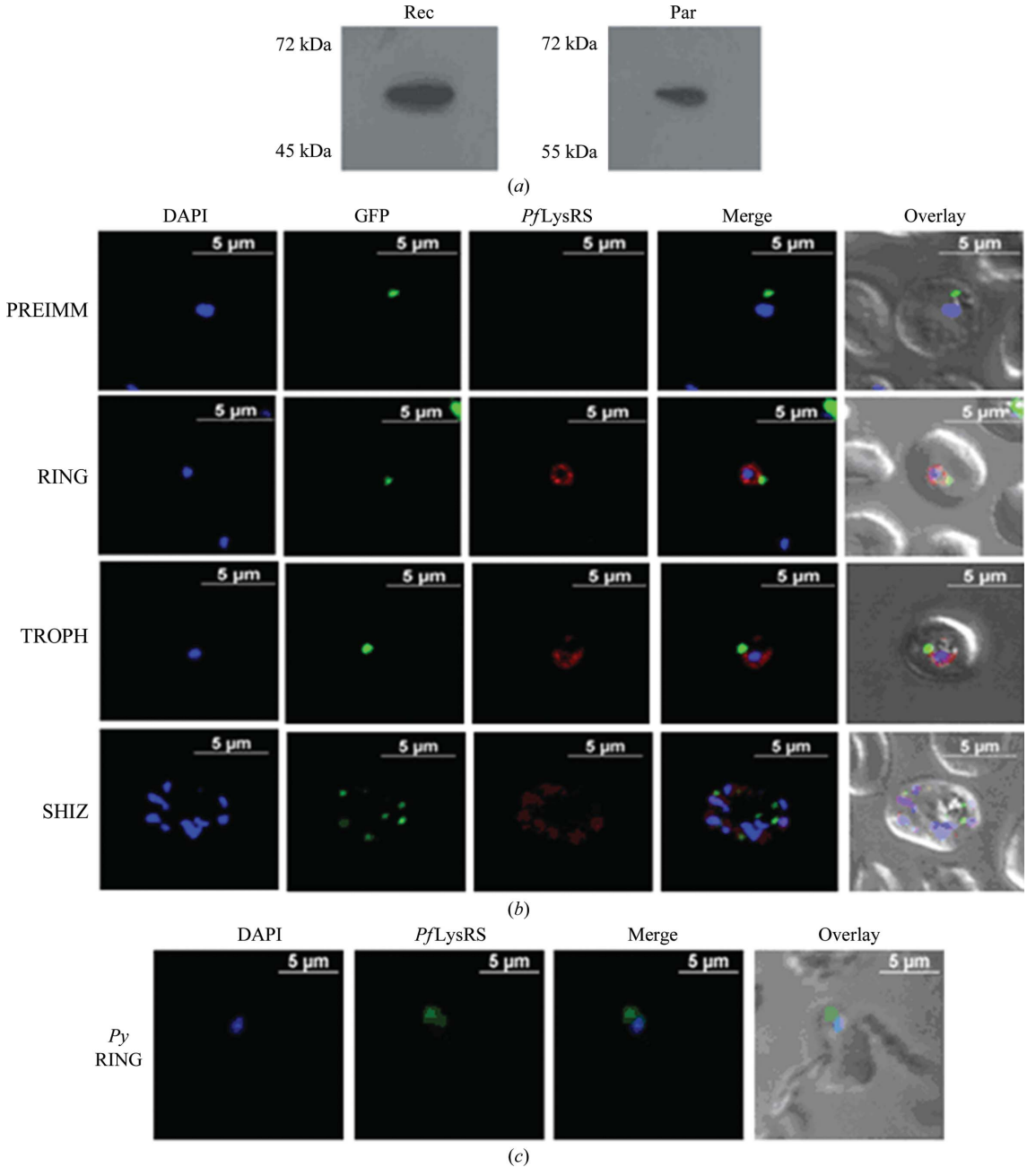

Figure 1
Expression and localization of *Pf*LysRS. (*a*) Western blot analysis of *Pf*LysRS expression in malaria parasites (Par) and of recombinant truncated *Pf*LysRS (Rec). (*b*) Localization of *Pf*LysRS in different intra-erythrocytic stages of *P. falciparum* by confocal immunofluorescence. The ring stage (RING), trophozoite stage (TROPH) and schizont stage (SHIZ) are shown and *Pf*LysRS is cytoplasmic in all stages. Preimmune sera (PREIMM) were used as a control. Each panel shows an image of cells stained with DAPI (blue); the parasite line used was GFP-tagged (strain D10 ACPleader-GFP), where apicoplast fluoresces green and anti-*Pf*LysRS antibodies fluoresce red. (*c*) *In vivo* localization of *Py*LysRS with anti-*Pf*LysRS antibodies in trophozoite stages of *P. yoelii*.

Table 1
X-ray diffraction data and structure-refinement statistics.

Data collection	
Wavelength (Å)	0.9537
Crystal-to-detector distance (mm)	275
Exposure time (s)	60
No. of frames	720
Unit-cell parameters (Å, °)	a = 141.3, b = 59.1, c = 297.2, α = 90, β = 97.5, γ = 90
Space group	$P2_1$
Resolution (Å)	50.0–2.91 (2.96–2.91)
Unique reflections	103775 (5229)
Multiplicity	4.1 (4.0)
Completeness (%)	95.1 (95.6)
$\langle I/\sigma(I)\rangle$	15.6 (4.1)
R_{merge}	0.10 (0.40)
Refinement	
Resolution (Å)	50.0–2.91
Reflections in work set/test set	103774/3110
R_{work}/R_{free} (%)	22.6/29.8
Model composition	
No. of protein atoms/waters	30748/97
Stereochemistry	
Bond lengths (Å)	0.10
Bond angles (°)	1.30
Ramachandran plot (%)	
Residues in allowed regions	99.4

recombinant *Pf*LysRS was confirmed by Western blot analysis, in which both the lysate and recombinant material revealed one band for *Pf*LysRS but at different sizes, as expected (Fig. 1*a*). A larger size band was observed (∼65 kDa) in the parasite lysate in line with gene annotation for *Pf*LysRS. The recombinant *Pf*LysRS migrated at ∼55 kDa, as expected from the truncated DNA construct (Fig. 1*a*). For microscopy, the parasites were co-stained with DAPI and GFP marker (for apicoplast) and we did not observe an overlap of fluorescence emanating owing to protein detection, indicating absence of *Pf*LysRS from the parasite nucleus and its apicoplast (Fig. 1*b*). Our results clearly show cytoplasmic localization of *Pf*LysRS in all the asexual life stages of the parasite (Fig. 1*b*), thus suggesting that this enzyme contributes to the production of lysyl-adenylate in parasite cytoplasm (and is distinct from the apicoplastic LysRS activity). Similar results were obtained when confocal microscopy was performed with *P. yoelii*-infected mouse red blood cells (Fig. 1*c*). The cytoplasm-localized *Pf*LysRS showed evenly spread staining in the parasite cytoplasm as judged by visual analyses and volumetric examination of z-stacks by confocal microscopy. Confocal IFAs with pre-immune sera and an antihistidine tag failed to produce fluorescence, validating the specificity of *Pf*LysRS antibodies (Fig. 1*b*). No signals were observed for *Pf*LysRS at the infected RBC membrane under normal growth conditions, suggesting a lack of *Pf*LysRS secretion from the parasite. This suggests differences between *Pf*LysRS and human counterpart enzyme in terms of noncanonical functions of LysRSs.

3.2. Crystal structure of *Pf*LysRS

Like other eukaryotic LysRSs, *P. falciparum* LysRS contains an N-terminal extension (residues 1–76) in its polypeptide sequence. In this study, the truncated *Pf*LysRS domain (residues 77–583) was cloned, expressed, purified and

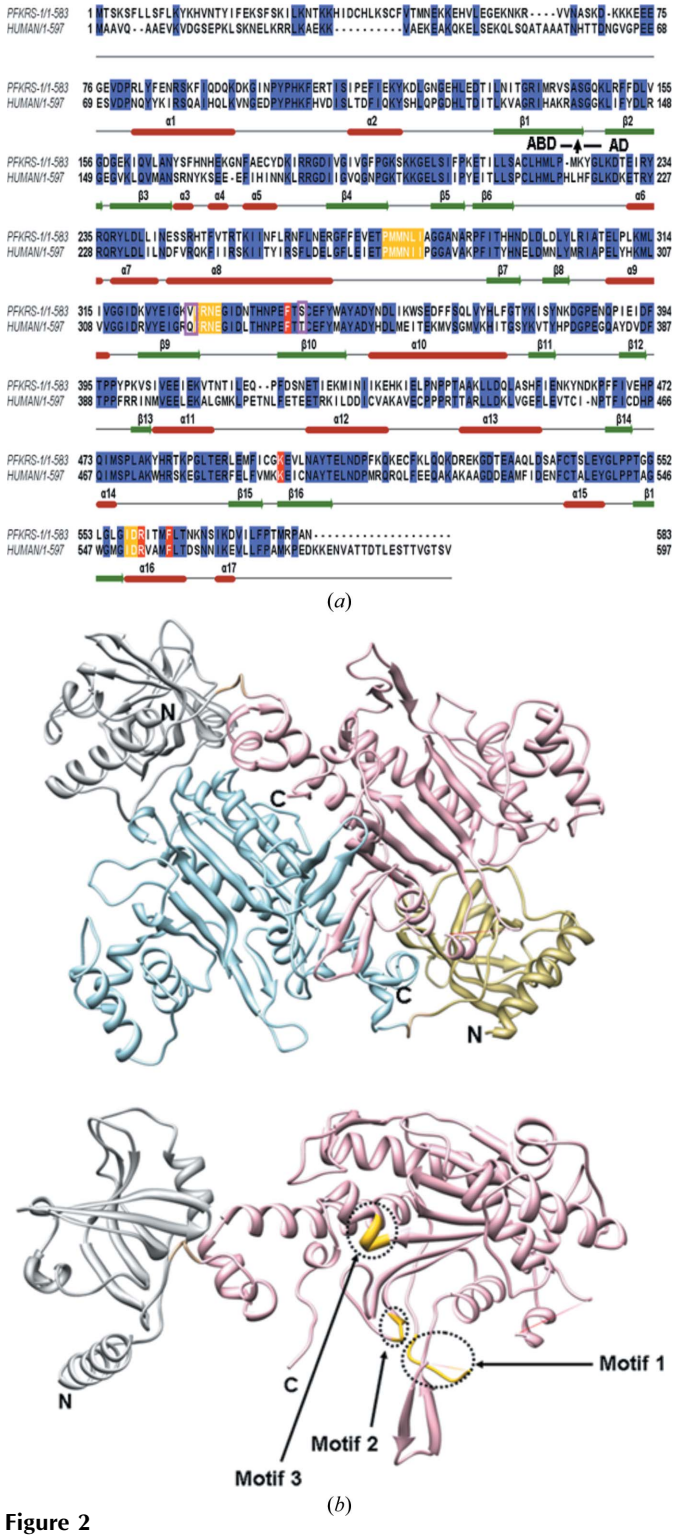

Figure 2
(*a*) Sequence alignment of class II LysRSs from *P. falciparum* (PFKRS-1) and human. The secondary-structure elements in the crystal structure of *Pf*LysRS are shown at the bottom. The domain consisting of residues 77–222 represents the anticodon-binding domain (ABD) and the C-terminus represents the aminoacylation domain (AD; residues 227–583). Active-site motifs (1, 2 and 3) are highlighted in yellow. Four residues (Phe342, Arg559, Lys499 and Phe563) of *Pf*LysRS that are likely to be involved in conformational changes are shown in red. (*b*) Overall structure of *Pf*LysRS in the apo form; ABD is in dark grey and AD is in pink. Monomers that form the dimer are shown, along with an image of the monomer alone with motifs 1, 2 and 3 highlighted in yellow.

used for crystallization. *Pf*LysRS crystals were obtained at 293 K by the hanging-drop vapour-diffusion method using 1 µl *Pf*LysRS (13.5 mg ml^{-1}) and 1 µl 0.1 *M* bis-tris pH 6.5, 2%(*v*/*v*) Tascimate pH 6.0, 20%(*w*/*v*) PEG 3350 at 293 K over a period of ∼15 d. We were unable to see any electron density for ATP and L-lysine and therefore the *Pf*LysRS apo form (*i.e.* unliganded enzyme) is discussed in the following. The structure of *Pf*LysRS was solved by molecular replacement using the crystal structure of human LysRS (PDB entry 3bju; Guo *et al.*, 2008) as the search model. The structure was refined at 2.9 Å resolution using the native data set. The crystals belonged to space group $P2_1$, with four dimers of *Pf*LysRS in the asymmetric unit and a solvent content of ∼56% (Table 1). *Pf*LysRS exists as a homodimer in the crystals (based on packing considerations). A structure-based multiple sequence alignment between *P. falciparum* and human LysRSs revealed 55% identity and showed few regions of sequence divergence (Fig. 2*a*). The overall structure of *Pf*LysRS (monomer) consists of 17 β-strands and 17 α-helices (Figs. 2*a* and 2*b*). The structure of each monomer harbours the N-terminal OB-fold anticodon-binding domain (Glu77–Pro222, shown in grey in Fig. 2*b*) and a C-terminal catalytic domain (Leu227–Pro581, shown in pink in Fig. 2*b*; the regions between, 282–288 and 514–538, are disordered in the structure). The catalytic domain displays typical conservation of motifs 1, 2 and 3 (Fig. 2*b*).

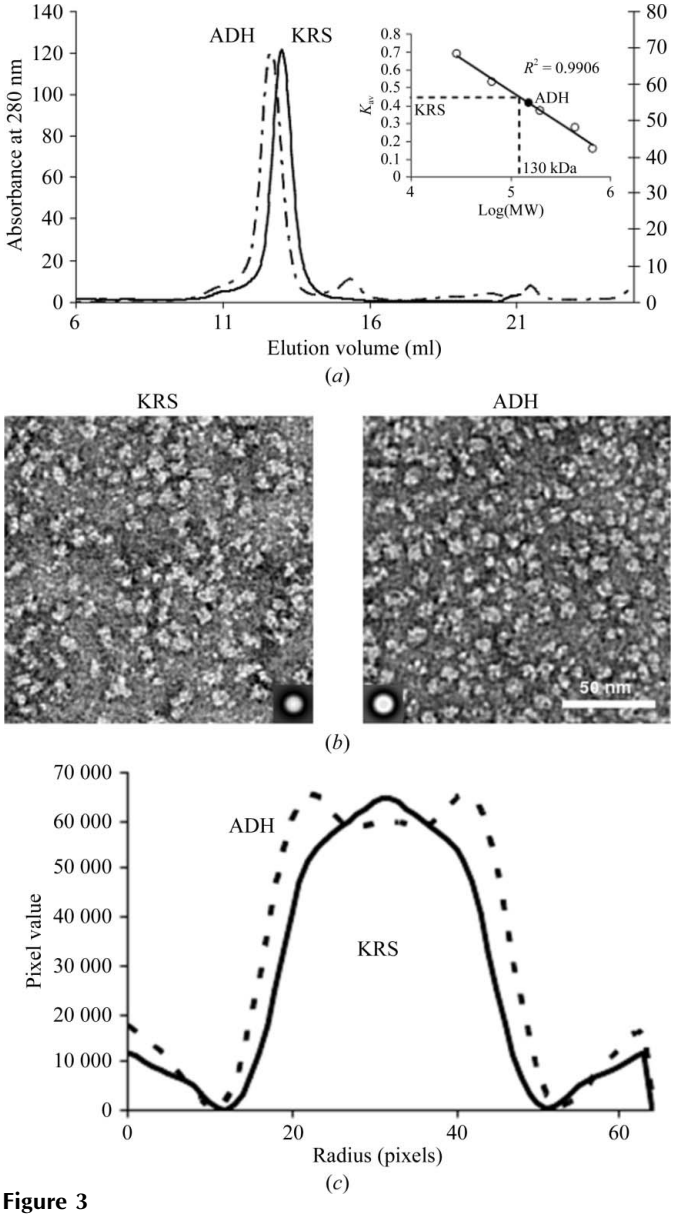

Figure 3
Oligomeric state of *Pf*LysRS (KRS) in solution. (*a*) Comparison of the size-exclusion elution profiles of *Pf*LysRS and the similarly sized yeast alcohol dehydrogenase (ADH). (*b*) Electron micrographs comparing the particle sizes of negatively stained *Pf*LysRS (left) and ADH (right). (*c*) Radial averages of ∼300 summed particle images from each micrograph are shown as insets. Plots of the radial profiles of averaged particle images of *Pf*LysRS and ADH are shown for comparison.

3.3. Comparison with human LysRS

The structure of *Pf*LysRS resembles that of human LysRS (*Hs*LysRS; the r.m.s.d. between 464 C^{α} atoms is ∼2.3 Å). To date, only one eukaryotic LysRS structure (from humans) is available in the PDB; we nonetheless compared *Pf*LysRS with both bacterial and human LysRSs. A prominent difference between bacterial/parasitic LysRSs and the human enzyme seems to be in their oligomeric states. *Pf*LysRS exists as a dimer in solution, while human LysRS seems to form dimers and tetramers (Guo *et al.*, 2008; Fang *et al.*, 2011). In the case of *Pf*LysRS crystals, no molecular contacts were evident that can build a tetramer interface as suggested for human LysRS (Guo *et al.*, 2008; Fang *et al.*, 2011). We confirmed the dimeric state of *Pf*LysRS using both gel-filtration chromatography (GPC; Fig. 3*a*) and negative-stained electron microscopy (Figs. 3*b* and 3*c*). Tetrameric alcohol dehydrogenase (ADH, ∼37 kDa per subunit) was used to calibrate the GPC. ADH migrated as expected at 150 kDa and the migration of *Pf*LysRS (55 kDa per subunit from SDS–PAGE) again suggested a dimeric structure of ∼130 kDa. From our analysis, it seems that the N-terminal extension of 76 residues is not required for dimer formation of *Pf*LysRS; indeed, it seems unlikely that the presence of the N-terminal extension of 76 residues contributes to tetramer formation. We mapped key residues from human LysRS onto *Pf*LysRS to investigate the structural basis for oligomer formation in these enzymes. For reference, a structural superposition of *Pf*LysRS and *Hs*LysRS using their anticodon-binding and catalytic domains is shown in Fig. 4. We have highlighted the human LysRS tetramer interface regions 1 and 2 and the apparently specific eukaryotic insertions 1 and 2 (Fig. 4). All of these regions are exposed on the protein surfaces of LysRSs (Supplementary Fig. S1[1]). However, they do not contribute to oligomer (tetramer) formation in *Pf*LysRS (Fig. 4). Our analysis suggests that although there is partial conservation in the interface and insertion residues between human and *Pf*LysRS, the latter does not exist as a tetramer (Fig. 4). In summary, we did not observe *Pf*LysRS tetramers as judged by three different sets of experimental

[1] Supplementary material has been deposited in the IUCr electronic archive (Reference: DW5034). Services for accessing this material are described at the back of the journal.

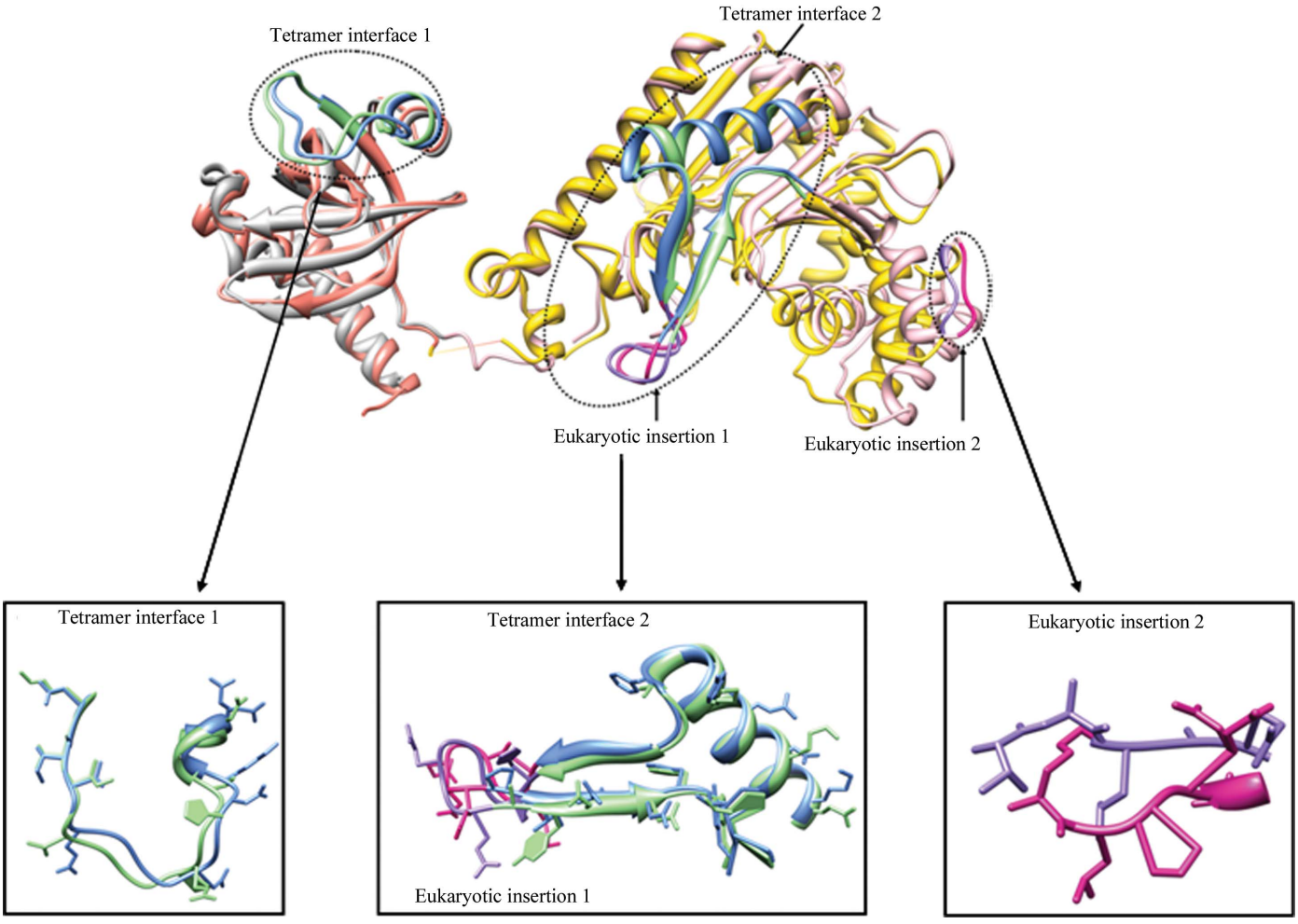

Figure 4
Structural comparison of monomers of *Pf*LysRS and *Hs*LysRS with their anticodon-binding domains (*Pf*LysRS, grey; *Hs*LysRS, plum; r.m.s.d. ∼1 Å) and catalytic domains (*Pf*LysRS, pink; *Hs*LysRS, yellow; r.m.s.d. ∼1.6 Å) superimposed. The tetramer interface 1 and 2 residues (*Pf*LysRS, green; *Hs*LysRS, blue) along with the specific eukaryotic insertion residues 1 and 2 (*Pf*LysRS, purple; *Hs*LysRS, deep pink) are highlighted in the insets.

data: crystal packing, gel-filtration chromatography and electron microscopy (Figs. 3 and 4). Finally, the purified fractions of *Pf*LysRS dimers readily aminoacylated *in vitro*-transcribed *Pf*tRNA^{Lys}, suggesting that the dimeric state of *Pf*LysRS is sufficient for enzymatic activity (Supplementary Fig. S2).

3.4. The malarial LysRS is capable of synthesizing Ap4a

Lysyl-tRNA synthetases (LysRSs) have previously been found to synthesize diadenosine tetraphosphate (Ap4a) using ATP as a substrate (Lee *et al.*, 1983; Varshavsky, 1983). We therefore tested the ability of *Pf*LysRS to synthesize Ap4a from ATP in the presence of L-Lys, ATP and Zn^{2+}. As shown in Fig. 5(*a*), upon the addition of *Pf*LysRS ATP was readily converted to a large-size molecule consistent with Ap4a. *Pf*LysRS was able to trigger Ap4a formation both in the presence and absence of L-Lys (Fig. 5*a*). We then identified all amino-acid residues that interact with Ap4a using the crystal structure of the complex of *Bacillus stearothermophilus* LysRS (*Bs*LysRS) with Ap4a (PDB entry 3a74; H. Sakurama, T. Takita, B. Mikami, T. Itoh, K. Yasukawa & K. Inouye, unpublished work). We mapped these Ap4a-interacting residues onto the *Pf*LysRS structure (Fig. 5*b*). It is evident from this analysis that most of the Ap4a-interacting residues are conserved between *Bs*LysRS and *Pf*LysRS, thus validating our experimental observations of Ap4a production by *Pf*LysRS. To our knowledge, this is the first report of the production of Ap4a by a malaria-parasite enzyme. Several previous studies have demonstrated that the concentration of Ap4a increases after the exposure of cells to various forms of metabolic stress such as heat, oxidation, nutritional and DNA damage (Lee *et al.*, 1983; Varshavsky, 1983). Ap4a molecules have therefore been described as 'alarmones' during cellular and metabolic stress conditions in prokaryotes (Lee *et al.*, 1983; Varshavsky, 1983). The significance of the production of Ap4a by malaria-parasite *Pf*LysRS remains to be explored in terms of its effect on parasite and host cells.

3.5. Interactions between ATP and LysRSs

We crystallized *Pf*LysRS in an apo (unliganded) form. To investigate the mechanism of ATP binding in the active site of

*Pf*LysRS, we directly compared the atomic structures of apo *Pf*LysRS and ligand-bound *Hs*LysRS. As is evident from Fig. 6(*a*), four side chains in ligand-bound *Hs*LysRS occur in favourable orientations (Phe335, Arg553, Lys493 and Phe557) and create a pocket for binding of the adenine ring of ATP (Fig. 6*a*). However, we observed that in the *Pf*LysRS structure the invariant side chains of Phe342, Arg559, Lys499 and Phe563 are in different rotameric states such that engagement with adenine will not be feasible unless there is a significant steric clash (Fig. 6*a*). Indeed, the asymmetric unit of *Pf*LysRS contains eight monomers (arranged as four dimers) and in most monomers the four side chains mentioned above (Phe342, Arg559, Lys499 and Phe563) have identical rotameric conformations (Fig. 6*b*) that would disallow binding to ATP. The residue Arg559 has two conformations in monomer chain *A* (Fig. 6*b*) and a different conformation in monomer *D*. This analysis indicates that *Pf*LysRS monomers within the crystal remain in a state which is not amenable to binding ATP owing to potential steric clashes. We therefore suggest that a series of small but definite conformational changes (*i.e.* rotameric alterations) must occur for ATP to bind in the active-site pocket of *Pf*LysRS (Fig. 6*a*). This observation is validated when the liganded and unliganded forms of all LysRS structures are compared with respect to the positions of the four key side chains that we have discussed above. For example, investigation into the structural states of the unliganded and ligand-bound forms of LysRSs from *E. coli* reveals no significant rotameric alterations in the equivalent residues to the four key residues (Phe342, Arg559, Lys499 and Phe563) that we have highlighted in *Pf*LysRS (Supplementary

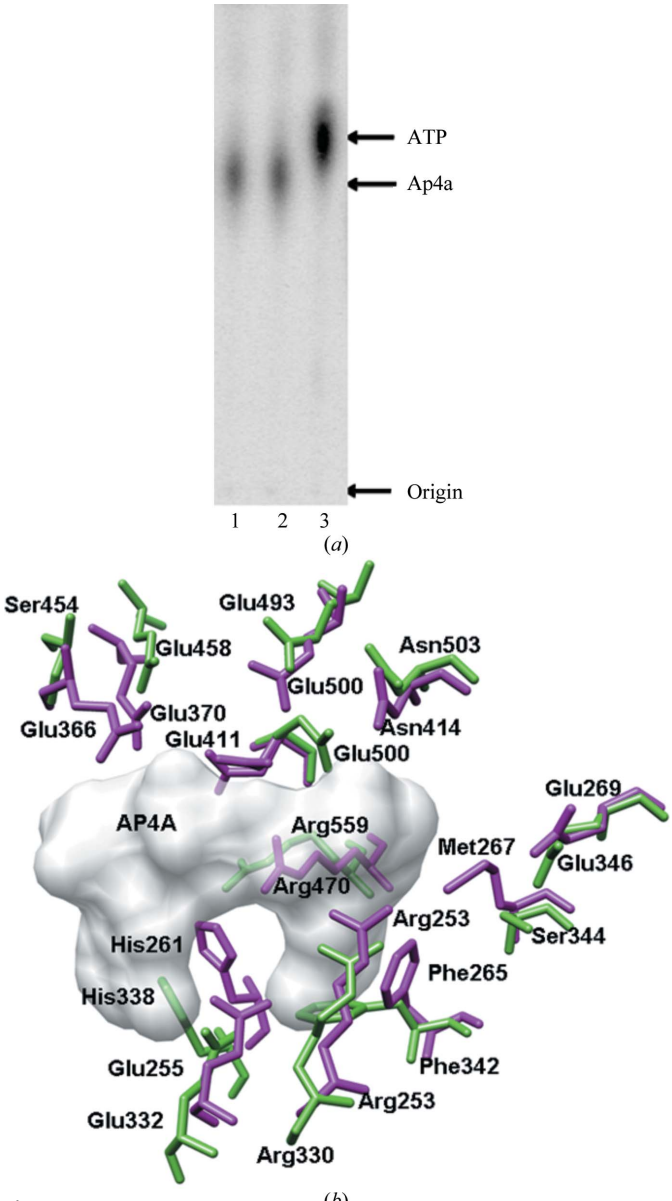

Figure 5
Ap4a synthesis. (*a*) One-dimensional resolution of Ap4a using [^{32}P]-labelled ATP and *Pf*LysRS; lanes 1 and 2 are reactions with and without L-lysine, respectively. Lane 3 contains [^{32}P]-labelled ATP only. (*b*) Superposition of *Bs*LysRS (*B. stearothermophilus*) complexed with Ap4a and *Pf*LysRS. Ap4a is shown as a molecular surface (grey), while the side chains of *Bs*LysRS and *Pf*LysRS are shown in magenta and blue. Most of the coordinating side chains are conserved between *Bs*LysRS and *Pf*LysRS. Residues with Ap4a-interacting side chains and those within 5 Å are highlighted.

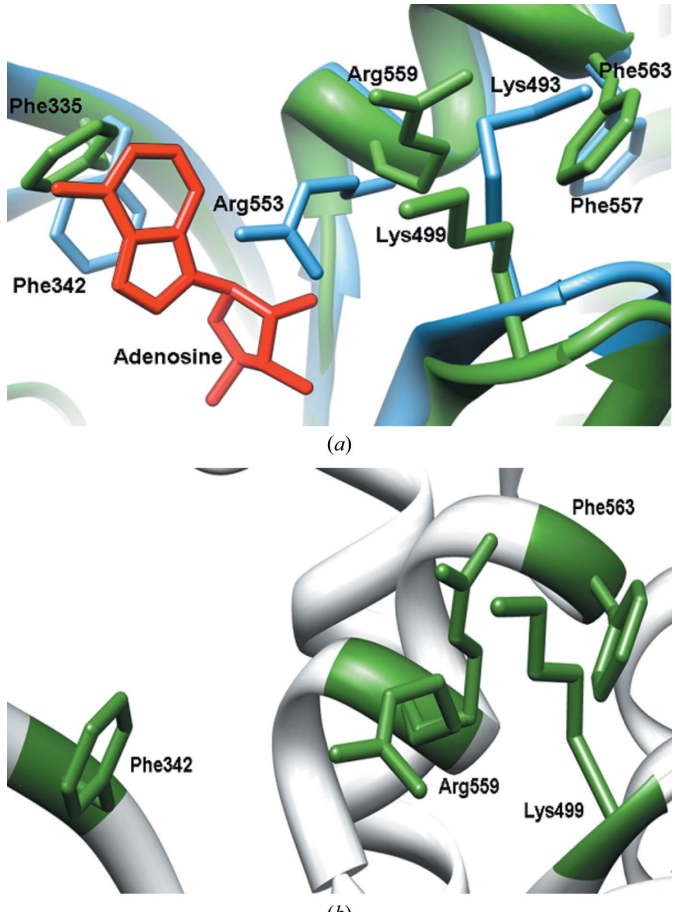

Figure 6
Active-site architecture of *Pf*LysRSs. (*a*) Superposition of *Hs*LysRS (closed, blue) and *Pf*LysRS (open, green) forms suggests that conformational changes in these four residues in *Pf*LysRS will be necessary before ATP can bind. We have removed the phosphates from ATP (red) for simplicity. (*b*) The *Pf*LysRS crystal asymmetric unit contains eight monomers (arranged as four dimers); only Arg559 was found to adopt multiple conformations.

Fig. S3). This analysis suggests that local structural alterations in key side chains of LysRSs contribute to the transition from unliganded to ligand-bound forms. Indeed, we thoroughly analyzed all 18 LysRSs in the PDB and it was striking to note that in all 18 cases (i) their radii of gyration fall within ∼1 Å and (ii) the r.m.s.d. only ranges from ∼2.3 to 3.2 Å. These comparisons suggest a lack of significant conformational changes at a global level within the overall structures of LysRSs irrespective of ATP occupancy. Overall structural conservation between monomeric bacterial, parasitic and human LysRSs is therefore high and ATP entry does not seem to cause exceptional conformational changes in bacterial or human LysRSs. Thus, dynamic flipping/rotameric samplings in the four key residues that we have highlighted above in *Pf*LysRS are the only significant structural differences that are evident in the crystal structures of bacterial, parasitic and human LysRSs. Together, these insights tend to support the conformational selectivity model of enzyme–substrate interactions (Changeux & Edelstein, 2011). However, further experimental validation is required to support this conclusion. Our analysis of the *Pf*LysRS active site suggests that the rotameric positions of Phe342, Arg559, Lys499 and Phe563 will be crucial for the entry and placement of the adenine ring of adenosine in a stacking format on top of Phe342 (Fig. 6*a*). In unliganded *Pf*LysRS the critical adenine-stacking Phe342 has an alternative rotamer which will disallow approach of the adenine ring of adenosine (Fig. 6*a*). A molecular-surface representation of these four residues in the ligand-bound *Hs*LysRS reveals a staircase-like stacking in which the adenine ring is inserted between the terminal Phe335 and Arg553 (Supplementary Fig. S4). In unliganded *Pf*LysRS, Phe342 is also stabilized by Arg559, Lys499 and Phe563 despite their presence in alternative rotameric conformations. Therefore, the residues we highlight in this analysis of *Pf*LysRS, Arg, Lys and Phe, seem to provide a lid on top of the key Phe342 which would eventually allow stacking of the adenine ring (Fig. 6*a*). In *Pf*LysRS, therefore, ATP engagement will favour conformational states in which the flipping of side chains of Phe342, Arg559, Lys499 and Phe563 allows the opening of a channel that lets adenine enter and dock onto Phe342 (Supplementary Fig. S4). The structural dynamics noted here will therefore not only enable the placement of adenine on top of the critical Phe (342 in *Pf*LysRS and 335 in human LysRS), but will also necessarily block the exit route for ATP once the closed (*i.e.* ligand-bound) conformation has been stabilized (Supplementary Fig. S4).

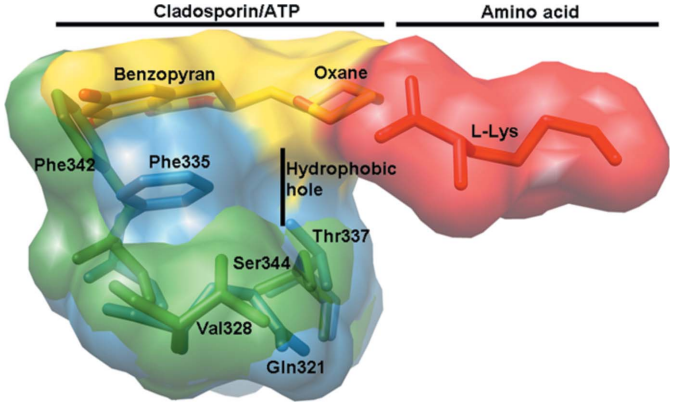

Figure 7
Molecular-surface view of key residues in the active sites of *Pf*LysRS (green) and *Hs*LysRS (blue) showing the hydrophobic hole in *Pf*LysRS which is absent in *Hs*LysRS. Cladosporin (yellow) and L-lysine (red) are shown in their respective binding pockets.

Based on the crystal structure of *Pf*LysRS, we validate previous observations (Hoepfner *et al.*, 2012) that cladosporin discrimination is based on the two aforementioned residues Val328 and Ser344 (Fig. 7). These smaller side chains in *Pf*LysRS clearly provide a larger hydrophobic cavity adjacent to the adenine-binding residue (Phe342) in *Pf*LysRS, into which the oxane ring of cladosporin fits more snugly (Fig. 7). From comparison of the molecular surfaces near the critical adenine/benzopyran-binding Phe residues in LysRSs (Fig. 7), it is evident that inhibitors with an extension of the oxane ring in the vicinity of the L-Lys-binding pocket within *Pf*LysRS can potentially provide a greater level of selectivity between human and malarial LysRSs (Fig. 7). Interestingly, the same two residues (equivalent to Val328 and Ser344 in *Pf*LysRS) are conserved in the related human malaria parasite *P. vivax*, thus suggesting that anti-LysRS drugs may be useful for other forms of human malaria.

4. Conclusion

Lysyl-tRNA^{Lys} can be synthesized by both class I (LysRS-I) and class II (LysRS-II) lysyl-tRNA synthetases using disparate active sites yet using similar strategies for substrate recognition (Terada *et al.*, 2002). *Pf*LysRS is akin to other eukaryotic LysRSs and belongs to the class II aaRSs. In general, tRNA synthetases (aaRSs) are increasingly being re-recognized as desirable targets for the development of antipathogen agents (Hurdle *et al.*, 2005; Bhatt *et al.*, 2009, 2011; Istvan *et al.*, 2011; Jackson *et al.*, 2011; Khan *et al.*, 2011; Hoepfner *et al.*, 2012). For instance, mupirocin is a selective inhibitor of malarial and bacterial isoleucyl-tRNA synthetases (Istvan *et al.*, 2011; Sheng & Zhang, 2011). Also, a broad-spectrum inhibitor of fungal leucyl-tRNA synthetases AN2690 is in development for the treatment of onychomycosis (Rock *et al.*, 2007). In line with this, *Pf*LysRS has recently been shown to be a good target for cladosporin, which is effective against both the liver and the blood stages of the parasite (Hoepfner *et al.*, 2012).

Our protein-expression data on *Pf*LysRS shows a full-length gene product with the expected protein molecular mass localized solely in the parasite cytoplasm (Fig. 1). Therefore, inhibition of this enzyme is expected to abrogate protein synthesis in the parasite cytoplasm only (distinct from apicoplastic tRNA charging). Our microscopy data also exclude the possibility of *Pf*LysRS secretion outside infected RBCs in the asexual stages of the parasite, a phenomenon that has been noted for human LysRS (Park *et al.*, 2005) and *Entamoeba histolytica* LysRS (Castro de Moura *et al.*, 2011). While the noncanonical functions of *Pf*LysRS remain to be explored, we show for the first time that the signalling molecule diadenosine

tetraphosphate (Ap4a) can be synthesized by *Pf*LysRS using ATP (Fig. 5*a*). Consistent with our experimental data on the conversion of ATP to Ap4a by *Pf*LysRS, we also note that the structural elements within LysRSs which bind Ap4a are highly conserved in *Pf*LysRS (Fig. 5*b*). In eukaryotic cells, it has been suggested that Ap4a plays a role in DNA replication (Lee *et al.*, 1983; Varshavsky, 1983). In the case of humans, LysRS is phosphorylated at a serine residue *via* the MAPK pathway following cellular activation (Yannay-Cohen *et al.*, 2009). Phosphorylated human LysRS is then released from the MSC such that it translocates into the nucleus, where it produces higher levels of Ap4a (Yannay-Cohen *et al.*, 2009). One profound effect of this Ap4a production is the removal of repressor Hint-1 from MITF, enabling it to transcribe its target genes (Yannay-Cohen *et al.*, 2009). These studied pathways have so far not been explored in malaria parasite biology, where homologues of Hint-1 and MITF are in any case lacking. We propose that given the absence of Hint-1 and MITF from the malaria genome, the production of Ap4a by malaria parasites (*via Pf*LysRS) is likely to have new and unexplored roles. In this vein, it is interesting to note that all malaria parasite genomes contain a gene that encodes diadenosine tetraphosphatase, which hydrolyses Ap4a, thus suggesting that the levels of Ap4a in the parasite need to be controlled by its own enzymatic machinery. In summary, given that malaria parasites have enzymes that both synthesize (*Pf*LysRS) and hydrolyze (diadenosine tetraphosphatase) Ap4a, control of its levels is clearly of importance for the pathogen.

Mechanistically, our structural analyses of LysRSs from bacterial, parasitic and human sources reveal interesting details about the engagement of ATP by this enzyme family. We found no evidence of large conformational changes between any of the bound and unbound states of the 18 LysRS structures available in the PDB. In fact, the r.m.s.d. values only vary between ∼2.3 and 3.2 Å and the radii of gyration between all 18 LysRS in the PDB are within ∼1 Å. This analysis rules out gross structural alterations in LysRSs upon engagement of ATP. Instead, we observed more subtle side-chain-based conformational variations in the ligand-binding pockets within the LysRSs, suggesting that different rotameric states of LysRSs exist even in the absence of ligand occupancy. This structural plasticity seems more consistent with the conformational selection model of enzyme action (Changeux & Edelstein, 2011).

For structure-based drug design, it is clearly important to exploit aaRS structures with differences between pathogen and human enzymes. The recent discovery of cladosporin (Hoepfner *et al.*, 2012) as a potent inhibitor of the asexual and the liver stages of malaria parasites bodes well for the development of a new generation of antimalarials based on *Pf*LysRS. We propose that chemical derivatization of cladosporin can focus on the oxane-ring part, which may be extended by adding new chemical groups that extend into the lysine-binding pocket of *Pf*LysRS (Fig. 7). In summary, our analysis of *Pf*LysRS provides structural data that can propel the development of improved antimalarial inhibitors.

We thank Dr Manickam Yogavel for help with structure refinement. SK is supported by the Council of Scientific and Industrial Research Fellowships (CSIR). AG and AKP are supported by the Department of Biotechnology (DBT), Government of India. This work was supported by the Department of Biotechnology, Government of India and by a Council of Scientific and Industrial Research fellowship. Research in the Ribas laboratory is supported by grant BIO2009-09776 from the Spanish Ministry of Education and Science. The Ribas and Sharma laboratories are supported by MEPHITIS grant 223024 from the European Union.

References

Abramoff, M. D., Magelhaes, P. J. & Ram, S. J. (2004). *Biophotonics Int.* **11**, 36–42.
Adams, P. D. *et al.* (2010). *Acta Cryst.* D**66**, 213–221.
Bhal, A., Brunk, B., Crabtree, J., Fraunholz, M. J., Gajria, B., Grant, G. R., Ginsburg, H. & Gupta, D. (2003). *Nucleic Acids Res*, **31**, 212–215.
Bhatt, T., Kapil, C., Khan, S., Jairajpuri, M., Sharma, V., Santoni, D., Silvestrini, F., Pizzi, E. & Sharma, A. (2009). *BMC Genomics*, **10**, 644.
Bhatt, T. K., Khan, S., Dwivedi, V. P., Banday, M. M., Sharma, A., Chandele, A., Camacho, N., de Pouplana, L. R., Wu, Y., Craig, A. G., Mikkonen, A. T., Maier, A. G., Yogavel, M. & Sharma, A. (2011). *Nature Commun.* **2**, 530.
Bochner, B. R. & Ames, B. N. (1982). *J. Biol. Chem.* **257**, 9759–9769.
Castro de Moura, M., Miro, F., Han, J. M., Kim, S., Celada, A. & Ribas de Pouplana, L. (2011). *PLoS Negl. Trop. Dis.* **5**, e1398.
Changeux, J.-P. & Edelstein, S. (2011). *F1000 Biol. Rep.* **3**, 19.
Chen, J. Z. & Grigorieff, N. (2007). *J. Struct. Biol.* **157**, 168–173.
Emsley, P. & Cowtan, K. (2004). *Acta Cryst.* D**60**, 2126–2132.
Fang, P., Zhang, H.-M., Shapiro, R., Marshall, A. G., Schimmel, P., Yang, X.-L. & Guo, M. (2011). *Proc. Natl Acad. Sci. USA*, **108**, 8239–8244.
Guo, M., Ignatov, M., Musier-Forsyth, K., Schimmel, P. & Yang, X.-L. (2008). *Proc. Natl Acad. Sci. USA*, **105**, 2331–2336.
Hoepfner, D. *et al.* (2012). *Cell Host Microbe*, **11**, 654–663.
Hurdle, J. G., O'Neill, A. J. & Chopra, I. (2005). *Antimicrob. Agents Chemother.* **49**, 4821–4833.
Ibba, M., Losey, H. C., Kawarabayasi, Y., Kikuchi, H., Bunjun, S. & Söll, D. (1999). *Proc. Natl Acad. Sci. USA*, **96**, 418–423.
Ibba, M., Morgan, S., Curnow, A. W., Pridmore, D. R., Vothknecht, U. C., Gardner, W., Lin, W., Woese, C. R. & Söll, D. (1997). *Science*, **278**, 1119–1122.
Ibba, M. & Söll, D. (2000). *Annu. Rev. Biochem.* **69**, 617–650.
Istvan, E. S., Dharia, N. V., Bopp, S. E., Gluzman, I., Winzeler, E. A. & Goldberg, D. E. (2011). *Proc. Natl Acad. Sci. USA*, **108**, 1627–1632.
Jackson, K. E., Habib, S., Frugier, M., Hoen, R., Khan, S., Pham, J. S., Ribas de Pouplana, L., Royo, M., Santos, M. A. S., Sharma, A. & Ralph, S. A. (2011). *Trends Parasitol.* **27**, 467–476.
Khan, S., Sharma, A., Jamwal, A., Sharma, V., Pole, A. K., Thakur, K. K. & Sharma, A. (2011). *Sci. Rep.* **1**, 188.
Lee, P. C., Bochner, B. R. & Ames, B. N. (1983). *Proc. Natl Acad. Sci. USA*, **80**, 7496–7500.
O'Donoghue, P. & Luthey-Schulten, Z. (2003). *Microbiol. Mol. Biol. Rev.* **67**, 550–573.
Otwinowski, Z. & Minor, W. (1997). *Methods Enzymol.* **276**, 307–326.
Park, S. G., Kim, H. J., Min, Y. H., Choi, E.-C., Shin, Y. K., Park, B.-J., Lee, S. W. & Kim, S. (2005). *Proc. Natl Acad. Sci. USA*, **102**, 6356–6361.
Pettersen, E. F., Goddard, T. D., Huang, C. C., Couch, G. S., Greenblatt, D. M., Meng, E. C. & Ferrin, T. E. (2004). *J. Comput. Chem.* **25**, 1605–1612.
Rock, F. L. *et al.* (2007). *Science*, **316**, 1759–1761.

Sampson, J. R. & Uhlenbeck, O. C. (1988). *Proc. Natl Acad. Sci. USA*, **85**, 1033–1037.
Schulman, L. H. & Pelka, H. (1983). *Proc. Natl Acad. Sci. USA*, **80**, 6755–6759.
Sheng, C. & Zhang, W. (2011). *Curr. Med. Chem.* **18**, 733–766.
Terada, T., Nureki, O., Ishitani, R., Ambrogelly, A., Ibba, M., Söll, D. & Yokoyama, S. (2002). *Nature Struct. Biol.* **9**, 257–262.
Tonkin, C. J., vanDooren, G. G., Spurck, T. P., Struck, N. S., Good, R. T., Handman, E., Cowman, A. F. & McFadden, G. I. (2004). *Mol. Biochem. Parasitol.* **137**, 13–21.
Varshavsky, A. (1983). *Cell*, **34**, 711–712.
World Health Organization (2011). *World Malaria Report 2010*. Geneva: World Health Organization.
Yannay-Cohen, N., Carmi-Levy, I., Kay, G., Yang, C. M., Han, J. M., Kemeny, D. M., Kim, S., Nechushtan, H. & Razin, E. (2009). *Mol. Cell*, **34**, 603–611.